Near-Field Focusing in Two-Dimensional Space Enclosed by Arrays of Different Geometries

DORIS NÄSLUND
MASTER´S THESIS
DEPARTMENT OF ELECTRICAL AND INFORMATION TECHNOLOGY
FACULTY OF ENGINEERING | LTH | LUND UNIVERSITY

Near-Field Focusing in Two-Dimensional Space Enclosed by Arrays of Different Geometries

Doris Näslund

Department of Electrical and Information Technology
Lund University

Supervisor: Jiawang Li

Examiner: Buon Kiong Lau

October 21, 2024

Printed in Sweden
Tryckeriet i E-huset, Lund

Abstract

With the increasing demands for higher data rates and long-range wireless power transfer, the development of new methods is a necessary step to meet the heightened requirements. One such method is improving the infrastructure for wireless transmission through the use of large intelligent surfaces (LIS). To be one step closer to enabling the construction of such infrastructure, this study examines the properties of near-field focusing (NFF) in the context of LIS by simulating NFF where the focal point is surrounded by antenna elements. The elements are placed to create two-dimensional (2D) arrays shaped like a circle, triangle, square and rectangle, enclosing a plane where the focal point is placed. The focusing is achieved by using the conjugate-phase approach. The array's simulated performance is evaluated by considering three performance metrics of NFF, the maximal achieved amplitude of the electric field, the size of the -3 dB spot region and the sidelobe level (SLL).

The results show that depending on where on the enclosed plane the focal point is placed, all performance metrics are affected. When comparing the array configurations, there are differences in regards to how greatly the metrics vary depending on the placement of the focal point. When there are large differences in the distance between the focal point and the closest antenna elements, there are also differences in the studied metrics. It is concluded that it is the inverse proportionality between the amplitude of the electric field and the distance from the focal point to the antenna elements that gives rise to the observed differences. When equalizing the arrays' area, their performance are comparable. All regular geometries with equal area can therefore be considered viable for near-field focusing within the enclosed 2D space.

In general, arrays with smaller area and circumference result in higher maximal electric field amplitude, while the size of the -3 dB region is almost unchanged. The amplitudes of the sidelobes also increase for smaller arrays, but the difference in dBV/m between the maximal amplitude and the highest sidelobe (i.e. SLL) is often similar for all the studied array sizes.

Acknowledgements

I would like to thank Jiawang Li, my supervisor, and Buon Kiong (Vincent) Lau, my examiner, for their great insight, enthusiasm and guidance throughout the thesis work. With their help, I was given the chance to conduct this simulation study over the summer of 2024, a rare opportunity where I was also provided valuable perspectives on life in academia and an exciting summer, good memories of which will stay with me for a long time.

Common abbreviations and physical quantities used throughout the study

Near-field focusing	NFF
Sidelobe level	SLL
Large intelligent surface	LIS
Internet of Things	IoT
Sixth-generation	6G
Two-dimensional	2D
Three-dimensional	3D

Electric field	$\mathbf{E}(\mathbf{r}, t)$	[V/m]
Electric field in phasor form	$\mathbf{E}(\mathbf{r})$	[V/m]
Initial amplitude of an electric wave	E_0	[V/m]
Unit vector	$\mathbf{a}$	
Wavelength	λ	[m]
Time	t	[s]
Angular frequency	ω	[rad/s]
Wave vector	$\mathbf{k}$	[cycles/m]
Vector pointing to an arbitrary point in space	$\mathbf{r}$	[m]
Vector pointing to antenna element n	$\mathbf{r}_n$	[m]
Vector pointing to the focal point	$\mathbf{r}_f$	[m]
The focal point when placed on the x-axis	x_f	[m]

Table of Contents

List of Figures

List of Tables

Chapter 1

Introduction

1.1 Background

To tackle the ever-increasing demands for wireless data and wireless energy transfer, technological innovations are essential in creating infrastructures that can satisfy the future needs for wireless communication. A promising concept for meeting the requirements is the use of large intelligent surface (LIS), an active surface covered with a massive amount of antenna elements. The surface could be integrated in walls of buildings and other large surfaces, in areas where communication systems and internet-of-things (IoT) devices are present. Due to the close distance between the device and the LIS, the setup allows for high data rates and more efficient power transfer that could support IoT devices at a larger scale and enable sixth-generation (6G) mobile communication.

In order to maximize the power transfer from the LIS, the energy from the surface could be focused on a smaller region in space, at the receiving device. By adjusting the phase and amplitude of each antenna on the LIS, the electromagnetic waves can constructively superimpose at one or more points in space, thus creating focused regions that could be aimed at the devices. In the far-field context, this method of using antenna arrays to create angular regions in space with higher radiated power is called beamforming. But since the LIS would be installed so that the communicating device would be near the antenna elements, the term near-field focusing (NFF) arrays can be used to denote antenna arrays used for this purpose.

With the desire to utilize higher frequencies and new infrastructures such as LIS, the need for design methods customized for efficient near-field usage is critical. While there are a multitude of methods for beamforming and controlling the angular focusing region in the far-field, there are few methods to choose from when focusing in the near-field. The two most prominent methods for designing NFF arrays are the closed-form conjugate-phase approach and utilizing optimization algorithms to find the desired weights for each antenna element.

The essence of using the conjugate-phase approach is that the phase of electromagnetic waves from each element is adjusted so that all waves superimpose constructively by being in-phase at a focal point of our choosing. Adjusting the phase with this approach is not a new concept. It has for example been studied in [4] and [5] using a planar array of antenna elements, focusing at a point in space above the array. Despite this, there is no known study where the antenna elements are distributed in different directions around the focusing point, which would be a common case for large-scale LIS implementations. An enabling factor for LIS-based communication infrastructure would be better understanding of how the focusing region is affected by having it surrounded by the antenna elements. Studying the focusing region in this context would serve as a part of the foundational knowledge necessary for designing efficient wireless data and/or power transmission using LISs, and would be another step toward 6G and larger scale IoT systems.

1.2 Goal of the thesis

The goal of the thesis is to examine simulated performance of differently shaped NFF antenna arrays, where the focal point in surrounded by the antenna elements, using the conjugate-phase approach. To limit the scope of the study, only a 2D plane will be studied. The array elements are distributed on the xy-plane, and the resulting electric field will only be examined over the 2D region enclosed by the elements.

The arrays will be studied by comparing the maximal achieved amplitude of the electric field, the size of the -3 dB spot region, and the sidelobe level (SLL) for the different setups. The aim is to identify trends regarding above mentioned performance metrics in relation to the geometry of the array being used. Knowledge of the effects the array geometry has when focusing in the near-field could be used as a foundation for designing future studies on the topic.

1.3 Structure of the thesis

Chapter 2 (*Theory*) aims to provide fundamental knowledge necessary to understand the methodology, results, discussion and conclusions. In Chapter 3 (*Methodology*) the process of designing the Matlab-based simulator and assumptions used are described. The results and discussion are both presented in Chapter 4 (*Results and Discussion*). Results are presented and discussed in tandem, with the conclusions being summarised in Chapter 5, (*Summary*). Chapter 5 also suggests topics related to the study that were outside the scope of this study, but would be valuable for consideration in future research.

Chapter 2

Theory

This chapter covers relevant background knowledge necessary to understand the results of this study. First, a brief introduction to electromagnetic waves and wave propagation is given. This is followed by an introduction to antennas and arrays, as well as beamforming in the far-field. Finally, The use of antenna arrays for NFF is covered.

2.1 Electromagnetic waves and wave propagation

Electromagnetic waves can be defined by variations in electric and magnetic fields in time and space. Changes in the fields first occur near the source of the fields, and propagates outward in space over time. For a time-harmonic electric wave, a sinusoidal change in the electric field, the electric field $\mathbf{E}$ (in units of V/m) at some position in free space can be expressed by

$$\mathbf{E}(\mathbf{r}, t) = \mathbf{E}_0 \cos(\omega t - \mathbf{k} \cdot \mathbf{r}) = \mathrm{Re}[\mathbf{E}_0 e^{j(\omega t - \mathbf{k}\cdot\mathbf{r})}], \tag{2.1}$$

where $\mathbf{r}$ is the position vector, t is time, $\mathbf{E}_0 = E_0 \mathbf{a}_E$ contains the wave's amplitude E_0 and its polarization direction given by the unit vector $\mathbf{a}_E$, ω is the angular frequency, $\mathbf{k}$ is the wave vector and Re[ ] is a function that takes a complex number and returns only the real part. $\mathbf{k}$ can further be described as $\mathbf{k} = 2\pi/\lambda\ \mathbf{a}_k$ with λ being the wavelength and $\mathbf{a}_k$ is the unit vector pointing in the direction of the wave's propagation [1].

Whenever an electric wave propagates through space, a corresponding magnetic wave will also propagate in tandem with the electric wave. The magnetic field $\mathbf{B}$ for a magnetic wave corresponding to the electric wave in (2.1) can be derived as seen in (2.2)

$$\mathbf{B}(\mathbf{r}, t) = \frac{1}{\omega} \mathbf{k} \times \mathbf{E}(\mathbf{r}, t). \tag{2.2}$$

Since $\mathbf{k}$ and $\mathbf{E}(\mathbf{r}, t)$ are orthogonal, $\mathbf{B}(\mathbf{r}, t)$ is orthogonal to both $\mathbf{k}$ and $\mathbf{E}(\mathbf{r}, t)$.

The magnetic and electric wave are also in-phase and travel in the same direction [1]. Because of the close relationship between electric and magnetic waves, only the electric component will be analyzed when discussing electromagnetic waves in the rest of the study.

An alternative way of analysing electromagnetic waves, in the special case of time-harmonic signals, is to instead consider a phasor representation of the fields. Rewriting (2.1) gives

$$\begin{aligned} \mathbf{E}(\mathbf{r}, t) &= \mathrm{Re}[\mathbf{E}_0 e^{j(\omega t - \mathbf{k}\cdot\mathbf{r})}] \\ &= \mathrm{Re}[(\mathbf{E}_0 e^{-j\mathbf{k}\cdot\mathbf{r}}) e^{j\omega t}] \\ &= \mathrm{Re}[\mathbf{E}_s(\mathbf{r}) e^{j\omega t}] \\ \implies \mathbf{E}_s(\mathbf{r}) &= \mathbf{E}_0 e^{-j\mathbf{k}\cdot\mathbf{r}}, \end{aligned} \tag{2.3}$$

where $\mathbf{E}_s(\mathbf{r})$ is the phasor representation of the electric field for the wave expressed in (2.1). The phasor enables analysis of the electric field without the need to conciser time-varying properties [2]. This study makes heavy use of the phasor notation. When using phasor notation, the electric field will be written as $\mathbf{E}(\mathbf{r})$, as will be done henceforth.

2.2 Antennas and antenna arrays

Electromagnetic waves are emitted from some source in space. Such a source comes in the form of a conducting path where current can flow. Changes in the current flowing through a conductor results in time-varying electric and magnetic fields, emitting from the source as electromagnetic waves. The conductor that produces this effect is referred to as an antenna. While changes in the current through the antenna results in changes in the surrounding fields, it is also true that changes in the surrounding fields will cause the current in the antenna to change. Thus an antenna can be used both for transmitting and receiving electromagnetic waves [1].

Depending on the construction, an antenna can exhibit a wide array of different characteristics. Other than the physical geometry, one of the most important traits of an antenna is its radiation pattern. The radiation pattern describes in what directions the antenna will emit electromagnetic waves with higher or lower intensity in both ϕ- and θ-polarized components. The simplest radiation pattern an antenna can exhibit is if the intensity is uniform in all directions radial to the antenna. Such an antenna is considered to be isotropic, and is a purely theoretical construct. Another basic antenna is the dipole antenna, which is linearly polarized and has a radiation pattern where the field attenuates closer to the poles of the antenna. For a dipole antenna oriented along the z-axis, electric waves would be emitted with the same amplitude in all directions along the xy-plane, while the amplitude would ideally be zero along the z-axis [3].

2.2.1 Far-field, radiative near-field and reactive near-field

When analyzing how antennas emit electromagnetic waves, it is important to consider how far away the point of interest is from the antenna. This is because resulting the electric field has different properties depending on the distance to the antenna. How the regions with different properties are defined can differ between literatures, but in the context of this study, three different regions are defined. The regions are the far-field, the radiative near-field, and the reactive near-field [1].

The far-field is characterized in the context of multiple antenna elements being used. For an array of receiving antenna elements with an isotropic transmitter placed in the far-field, it can be assumed that the incoming electromagnetic waves are planar, i.e. they reach every antenna element from the same direction. This being despite the fact that spherical waves are emitted from the isotropic source. A common definition is that the far-field includes all points in space that satisfies $|\mathbf{r}| > 2D/\lambda$, with D being the largest physical dimension of the antenna. All other points closer to the antenna elements are considered to be within the near-field [1].

While the largest difference between the far-field and near-field is that incoming waves cannot be assumed to be planar in the near-field, the near-field itself can be divided into two regions. These regions are the radiative near-field and the reactive near-field, with the reactive near-field being closest to the antenna. The reactive near-field is characterised by complex electrodynamic interactions where energy can oscillate between the antenna and the surrounding space [1]. When considering a dipole antenna, this region can approximately be defined as all points in space that satisfies $|\mathbf{r}| < \lambda/2\pi$. However, it is important to note that there is no discrete boundary between the radiative and the reactive near-fields. Instead, there is a region of space with gradual change where both field characteristics are prevalent. To ensure that the radiative component dominates, it is therefore necessary to only consider points even further away than $|\mathbf{r}| = \lambda/2\pi$, e.g. distances of a couple of wavelengths away. In the radiative near-field, the amplitude of the electric field from a dipole antenna attenuates proportionally to the inverse of the distance to the point in space, also expressed in (2.4) [3].

$$|\mathbf{E}(\mathbf{r})| \propto 1/|\mathbf{r}|. \tag{2.4}$$

2.2.2 Beamforming in the far-field

Depending on the application, the radiation pattern of the antenna can be a vital parameter. It can for example be desirable to send electromagnetic waves with high amplitude in one direction, while the amplitude is lower in others. One way of achieving this is through beamforming [1].

The idea behind beamforming is that several antenna elements that are close in space are transmitting or receiving simultaneously. Due to constructive and destructive interference from each element, the electric field will exhibit larger oscillations in some regions in space, while the oscillations will be weaker in other regions. Far away from the antenna elements, the regions appear in beam-like shapes coming from the elements, hence the name beamforming. Steering the beam and changing the amplitude of oscillation for different regions in space can be achieved by adjusting the phase and amplitude of waves being transmitted or received from each antenna element. This is also referred to as assigning weights to the antenna elements [1].

A side effect when beamforming is that there will appear other regions in space where there is some partial constructive interference between the waves. These regions are referred to as sidelobes, and they are an unavoidable consequence of beamforming. An important factor when designing a beamformer is the intensity of the sidelobes and where the sidelobes appear. Larger distances between the antenna elements give rise to higher sidelobes. When using element separation larger than 0.5λ, there is also the possibility of so called, grating lobes being formed, sidelobes with amplitudes similar to that of the the main beam. By changing the element separation as well as phase and amplitude of each element, it is possible to control the sidelobes to fit design criteria. Often a balance must be found between qualities of the main beam and that of sidelobe suppression, depending on the application and limitations by the setup being considered [1].

2.3 NFF using the conjugate-phase approach

NFF arrays are antenna arrays used for beamforming in the near-field. Unlike in the far-field, the focusing region often does not appear in a beam-like shape (over the angular domain) when focusing in the near-field. Instead, a spatial region with more clearly defined width and depth will exhibit the greatest field strength. The position and shape of this region can be controlled by adjusting the weights of the antenna elements. Since the spherical waves cannot be approximated to be planar in the near-field, it is a more complicated procedure to control the focusing region when in the near-field. The differing distances and angles between the elements and points in space lead to more complex interactions compared to the far-field case. To our knowledge, using the conjugate-phase approach and optimizations algorithms are the only two ways to achieve a focusing region in the near-field around a point in space, called the focal point [4].

When using the conjugate-phase approach to design NFF arrays, only the phase of each element is weighted. The goal of the method is for the electromagnetic waves from each element to superimpose constructively with one another at a certain point in space. The phase of each element is individually adjusted to compensate for the differences in travel time to the focal point, thus ensuring that the waves will be in-phase at the focal point. Consider the electric field in the radiative near-field from a dipole antenna located in the origin, where the waves propagate radially from the antenna. The electric field can be described by combining (2.3) and (2.4), and can written as

$$\begin{aligned}\mathbf{E}(\mathbf{r}) &= \mathbf{E}_0 \frac{e^{-j\mathbf{k}\cdot\mathbf{r}}}{|\mathbf{r}|} \\ &= \mathbf{E}_0 \frac{e^{-j2\pi|\mathbf{r}|/\lambda}}{|\mathbf{r}|}.\end{aligned} \tag{2.5}$$

Using the conjugate-phase approach, the phase is adjusted so that $\mathbf{E}(\mathbf{r}) = \mathbf{E}_0/|\mathbf{r}|$ at the focal point. The vector describing the focal point is denoted as $\mathbf{r}_f$, and thus the phase shift ϕ can be adjusted and expressed as

$$\begin{aligned}\mathbf{E}(\mathbf{r}) &= \mathbf{E}_0 \frac{e^{-j2\pi|\mathbf{r}|/\lambda+j\phi}}{|\mathbf{r}|} \\ &= \mathbf{E}_0 \frac{e^{-j2\pi|\mathbf{r}|/\lambda+j2\pi|\mathbf{r}_f|/\lambda}}{|\mathbf{r}|} \\ &= \mathbf{E}_0 \frac{e^{-j2\pi(|\mathbf{r}|-|\mathbf{r}_f|)/\lambda}}{|\mathbf{r}|}.\end{aligned} \tag{2.6}$$

If the antenna element now labeled n is placed at an arbitrary point in space given by $\mathbf{r}_n$, the electric field can be expressed as

$$\mathbf{E}_n(\mathbf{r}) = \mathbf{E}_{0n} \frac{e^{-j2\pi(|\mathbf{r}-\mathbf{r}_n|-|\mathbf{r}_f-\mathbf{r}_n|)/\lambda}}{|\mathbf{r}-\mathbf{r}_n|}. \tag{2.7}$$

In (2.7), $|\mathbf{r}-\mathbf{r}_n|$ describes the distance between the antenna and an arbitrary point in space, and $|\mathbf{r}_f - \mathbf{r}_n|$ describes the distance between the antenna and the focal point. Finally, consider N antenna elements distributed at unique points in space. Using the conjugate-phase approach presented in (2.7), the total superimposed electric field at a point in space could be described as

$$\mathbf{E}(\mathbf{r}) = \sum_{n=1}^{N} \mathbf{E}_n(\mathbf{r}) = \sum_{n=1}^{N} \mathbf{E}_{0n} \frac{e^{-j2\pi(|\mathbf{r}-\mathbf{r}_n|-|\mathbf{r}_f-\mathbf{r}_n|)/\lambda}}{|\mathbf{r}-\mathbf{r}_n|}. \tag{2.8}$$

Notice how this phase adjustment ensures that $\mathbf{E}_n(\mathbf{r}) = \mathbf{E}_{0n}/|\mathbf{r} - \mathbf{r}_n|$ for all N elements when $\mathbf{r} = \mathbf{r}_f$. This is the essence of the conjugate-phase approach [4].

Chapter 3

Methodology

This study examines NFF antenna arrays where the elements are distributed along different 2D shapes enclosing the focal point. This chapter first describes the assumptions used for the simulations and analysis. Then the array geometries are introduced, followed by a description of how the performance of each setup was evaluated. Lastly the design of the simulations is also described in greater detail.

3.1 Prerequisites and assumptions

This study focuses only on comparing differently shaped 2D array configurations located on the xy-plane. To limit the scope of the study, the electric field was only simulated on the 2D plane that the elements was located on.

When simulating the electric field for the different arrays, the following assumptions and prerequisites were used. It was assumed that the waves were propagating through free space, and that $\lambda = 0.2$ m for all simulations. Analysis of the mutual coupling between the antenna elements was deemed to be outside of the scope of this study, and therefore it was not accounted for. The antenna elements were chosen to be modeled as z-polarized dipole antennas located in the xy-plane. This implied that they would radiate equally in all directions along the xy-plane, and the amplitude of the electric wave emitted by each element was set to one, i.e, $E_0 = 1$ V/m. These assumptions were made in order to better study how the shape of the array affects the focusing.

Because the antenna elements were modeled as z-polarized dipole antennas, the electric field from each element was linearly polarized along the z-axis ($\mathbf{a}_E = \mathbf{a}_z$), 90° from the wave's traveling direction along the xy-plane. Since all waves were linearly polarized in the same direction, their amplitudes could be summed to get the resulting field.

Because (2.8) is only valid in the radiative near-field, a boundary was decided upon that would separate the radiative and the reactive near-fields. Due to the space with gradual change between the fields, the boundary of $|\mathbf{r} - \mathbf{r}_n| = \lambda/2\pi$ was deemed to be tot close to the element. To make sure that there would be little to no remnants left from the reactive near field in the simulation space, 1.5λ was chosen as the boundary. Therefore, the electric field for all positions closer to the antenna than 1.5λ was not included in the results. $|\mathbf{r} - \mathbf{r}_n| = 1.5\lambda$ was chosen to be the boundary after doing test-simulations using (2.8) and with the knowledge that the radiative component clearly dominates a couple of wavelengths away from the element, as stated in [3]. It is possible that the proposed model for the electric field was valid for points even closer to the elements. But, to be able make that claim with confidence, a more in depth analysis of the reactive near-field would be necessary.

3.2 Antenna configurations

In order to compare the performance of the differently shaped NFF arrays, four general shapes were examined. The shapes that where studied was: a circle, an equilateral triangle, a square and a rectangle with two sides being three times as long as the two other sides. The arrays consisted of $N = 120$ z-polarized dipole antenna elements, evenly spaced out along the shapes. The reason as to why $N = 120$ elements were used is because it was a compromise between using as many elements as possible while keeping a reasonable element separation as well as not resulting in unreasonable simulation times. See Figure 3.1 for illustrations of the four arrays.

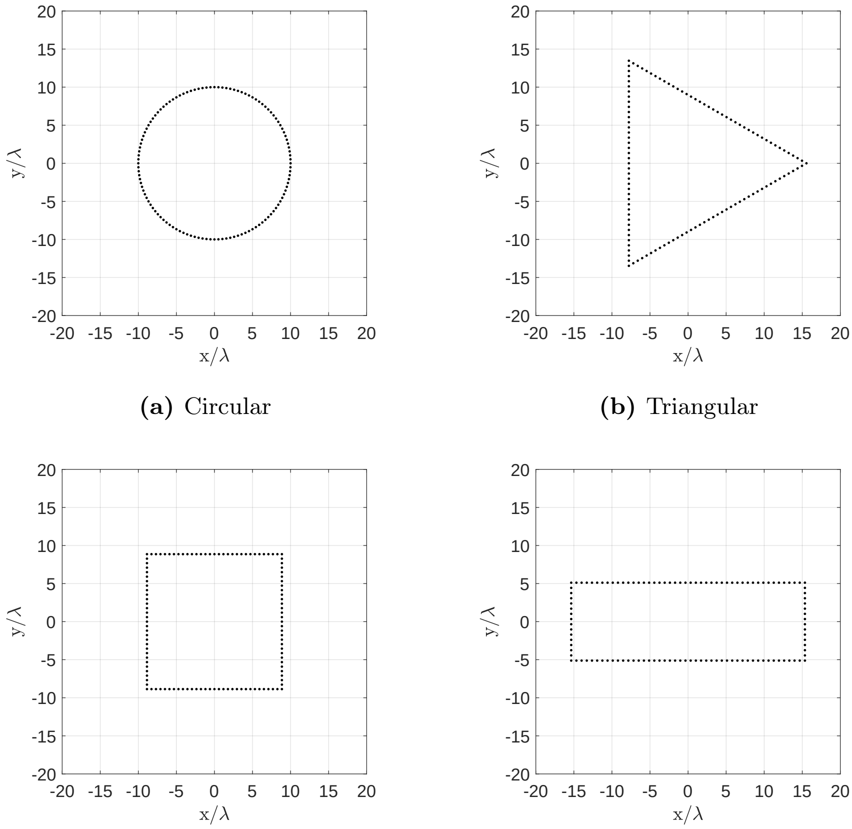

(a) Circular

(b) Triangular

(c) Square

(d) Rectangular

Figure 3.1: Planar arrays with equalized area consisting of $N = 120$ elements each, marked with black dots. The x and y coordinates of each element are scaled to the wavelength. For example, the diameter in (a) is 4 m, and using $\lambda = 0.2$ m results in the diameter being displayed as 4 m$/0.2$ m $= 20$ in the figure.

In order to create fair grounds for comparing the differently shaped arrays, some attribute of the shape was equalized. This attribute could in theory be arbitrary, but it was decided that the main analysis of the study would be done on the case where the area of all shapes was equalized.

There were several important factors to account for when deciding upon what this area would be. There would need to be sufficient space within the arrays to have as much of the enclosed area as possible to be within the radiative near field. On top of that, the element separation d was a critical factor to consider in this context. $d > 0.5\lambda$ was desirable since the mutual coupling between the elements could be safely neglected, as stated in [4]. But, as stated in [1], it is common knowledge in a far-field context that having $d > 0.5\lambda$ runs the risk of grating lobes being formed. This effect becomes amplified as d increases. Therefore, the circular array was decided to have the diameter 20λ in order to balance out these factors, resulting in $d = 0.52\lambda$ for the circular array. After the circular array had its area decided, the dimensions of the other arrays were calculated.

Because there was no clear best way of equalizing the arrays, results were also produced using different methods of equalization. These results were based upon equalizing the aperture of the arrays, and equalizing the circumference of the arrays. In this case, equalizing the aperture entailed that the longest length found across the array would be the same. Notable characteristics of the equalization methods were that equalizing the area yielded the largest aperture, circumference and element separation, while equalizing the aperture yielded the smallest area, circumference and element separation. See Tables 3.1(a)-(c) for an overview of the characteristics of the different arrays.

	A [m^2]	D [m]	C [m]	d/λ
Circular	12.57	4.000	12.57	0.52
Triangular	12.57	5.387	16.16	0.67
Square	12.57	5.013	14.18	0.59
Rectangular	12.57	6.472	16.37	0.68

(a) Equalizing the area.

	A [m^2]	D [m]	C [m]	d/λ
Circular	12.57	4.000	12.57	0.52
Triangular	6.928	4.000	12.00	0.50
Square	8.000	4.000	11.31	0.47
Rectangular	4.800	4.000	10.12	0.42

(b) Equalizing the aperture.

	A [m^2]	D [m]	C [m]	d/λ
Circular	12.57	4.000	12.57	0.52
Triangular	7.598	4.189	12.57	0.52
Square	9.870	4.443	12.57	0.52
Rectangular	7.402	4.967	12.57	0.52

(c) Equalizing the Circumference.

Table 3.1: Characteristics of arrays using different methods of equalization, calculated from the diameter of the circular array being equal to 20λ. A refers to the enclosed area, D refers to the longest length found across the array, C refers to the circumference and d refers to the elements separation. Notice that d/λ is scaled to $\lambda = 0.2$ m, where if $d = 0.104$ m, it would be presented as $d/\lambda = 0.104$ m$/0.2$ m $= 0.52$ in the table.

3.3 Evaluating simulated performance

In order to compare the different antenna configurations, their performance was evaluated by studying three performance metrics. These metrics were the maximal amplitude of the electric field, the -3 dB spot region and the SLL.

By evaluating the maximal achieved amplitude of the electric field, it was possible to compare the different arrays' ability to provide power to different regions in space. This would be relevant in a real-life context when constructing similar arrays. A receiver could be designed with knowledge of how the array geometry affects the power transfer, making it an important aspect to study.

The -3 dB spot region is defined as a region in space where the electric field amplitude is at most 3 dB less than that of the maximal amplitude. It is an attribute describing how large the space was where one could expect to be able to receive at least half of the maximal power found at the focal point. Hence, results showing a small -3 dB spot indicates that the electric field is more focused, while a larger -3 dB spot indicates that the electric field is close to the maximal amplitude for a larger region, thus being less focused.

In order to quantify the sidelobe behaviour, studying the sidelobes' amplitudes and where they were located is relevant for evaluating the arrays' performance. To quantify the SLL, this study examined the difference between the sidelobe with the highest amplitude and the maximal amplitude of the electric field. Since sidelobes often are an unwanted consequence, better SLL implies that there is a larger difference between the main lobe and greatest sidelobe. It is worth noting that this method gave no direct information regarding where the largest sidelobe was located. Due to time constraints, it was decided that the investigation of the sidelobes' locations would be done at a smaller scale than previously mentioned aspects. This investigation instead consisted of presenting a select few cases where the location of certain sidelobes became important for other results.

Another point that was examined was how the above mentioned factors not only are affected by which of the differently shaped arrays that is used, but also at what position inside the arrays the focal point is chosen to be in. It is clear by (2.4) that the contribution to the electric field from elements close to a point of interest is greater than for elements further away. Therefore, it was possible that the geometry of the array was more relevant for some points in space compared to others. It was of great interest to study how the performance of the NFF arrays are affected by where the focal point is placed. Several points inside each array was chosen as the focal point so as to capture the potential changes that could arise when moving the focal point across each array.

3.4 Designing the simulations

Matlab version R2024a was used for simulating the electric field and producing resulting figures, utilizing no toolbox. When simulating the electric field, (2.8) was used as the foundational mathematical model. Because of the potential changes that could depend on where the focal point was placed, simulations for the electric field was done for a number of focal points along the x-axis. The arrays were set up in such a way that the center of each array was located in the origin. This was to capture behaviours that corresponded to moving the focal point along the diameter of the circular array and along the line spanning the height of the triangular array. For the square and the rectangular arrays, more lines were examined. The square array was studied along both the line of symmetry parallel to the sides, and along the diagonal. As for the rectangular array, the two lines of symmetry parallel to the long and short sides were studied, as well as the diagonal. This resulted in a total of seven lines across all arrays that was examined.

When moving the focal point along the different lines for the square and rectangular arrays, the simulations were constructed in such a way that the lines were allays along the x-axis. To have the x-axis coincide with the desired line, the arrays and xy-plane were rotated. While this has no effect on the physics of the setup, it is important to keep in mind when interpreting the results. See Figure 3.2 for a plot depicting all simulated setups and lines for moving the focal point.

After each simulation, post processing was done convert to dBV/m, remove unwanted data for points outside the enclosed space and adhere to the the limitations of the model used. Since electric fields are proportional to square roots of power quantities, the amplitude was converted to dBV/m using $\mathbf{E}(\mathbf{r})$ [dBV/m] $= 20 \cdot \log_{10}(\mathbf{E}(\mathbf{r})$ [V/m]). Because (2.8) is only applicable in the radiative near-field, all simulations where at least one point of the -3 dB spot region satisfied $|\mathbf{r} - \mathbf{r}_n| < 1.5\lambda$ were removed. This was done because the spot was deemed to not satisfy the prerequisites for the model, and thus could not be used to calculate the size of the -3 dB spot. For the remaining simulations, the electric field at all points where $|\mathbf{r} - \mathbf{r}_n| < 1.5\lambda$ where ignored in the analysis for the same reason.

For each focal point along the x-axis, the electric field was simulated on an area defined by the antenna elements' maximal x and y positions on the xy-plane. These results were used to find the maximal amplitude of the electric field and the SLL. These results were extracted by finding peaks in the data describing the electric field, where the highest peak corresponded to the maximal achieved amplitude of the electric field and the second highest corresponded to the highest amplitude of the sidelobes. When evaluating the size of the -3 dB spot region, it would have been necessary to use a resolution that was higher than what was possible with the script and computer used to produce usable results. Therefore, a separate simulation was set up where the simulation area only covered the lines passing through the focal point pointing in the $\mathbf{a}_x$ and $\mathbf{a}_y$ directions. The spot's size was extracted through, by starting at the focal point, seeing how far along the $\pm\mathbf{a}_x$ and $\pm\mathbf{a}_y$ directions the electric field at point p satisfied $|\mathbf{E}(\mathbf{r}_p)| > \text{Max}(|\mathbf{E}(\mathbf{r})|) - 3$. The size of the spot is therefore presented as the length of the spot in the $\mathbf{a}_x$ and $\mathbf{a}_y$ directions, passing through the focal point.

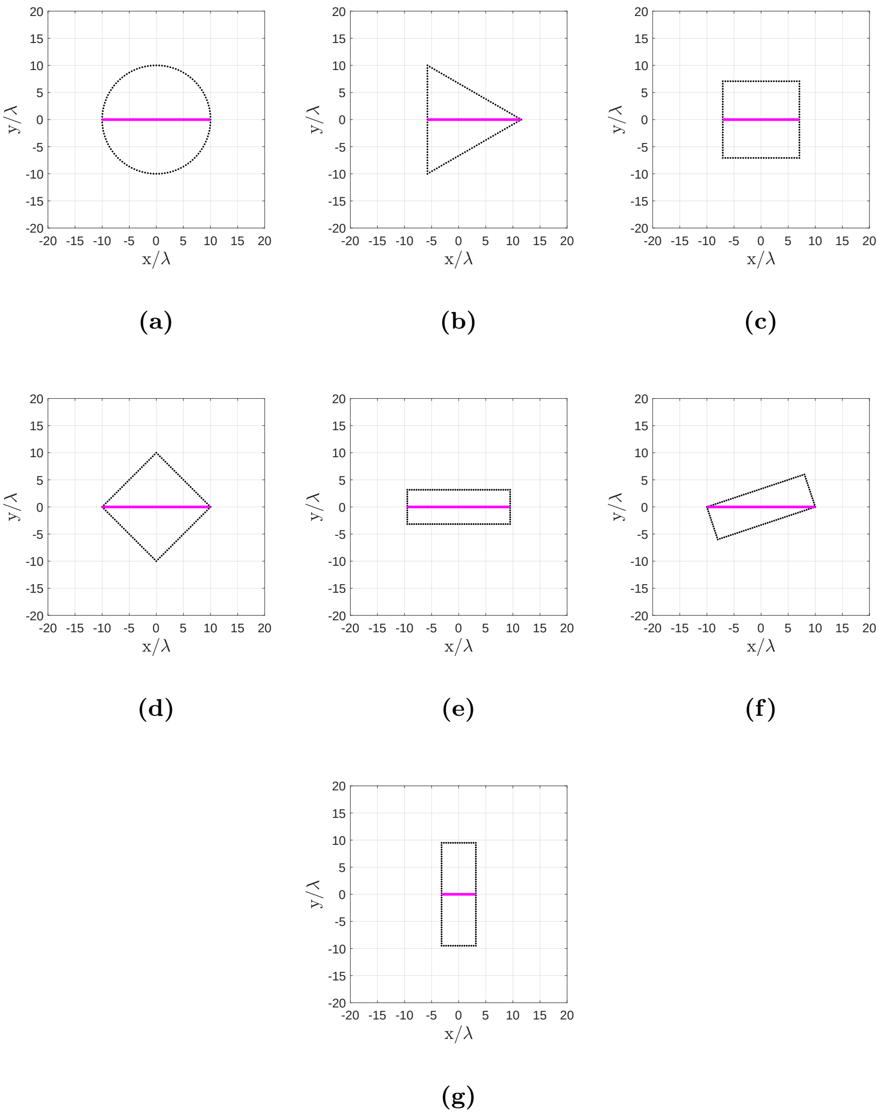

Figure 3.2: Depictions of all setups used for simulation, including the rotated square and rectangular arrays. The line for which the focal point was moved along is colored magenta.

Chapter 4

Results and discussion

In this chapter, results produced by the simulation setups described in Chapter 3 are presented and analyzed. First, for the different array geometries, the maximal amplitude of the electric field is examined, followed by the -3 dB spot region. The chapter ends with results and discussion regarding the SLL. This chapter primarily focuses on results produced when equalizing the arrays' area, and only covers the alternatives briefly or when relevant. Detailed results for cases where array aperture and circumference were equalized are included in Appendix A and should be viewed as complementary to the results presented in this chapter.

When presenting the results, the results for all simulations using the same geometry is overlaid in the same figure. This is relevant for interpreting the square and rectangular array. To distinguish the results from the different simulations, results from using the square array setups seen in Figures 3.2(c) and (d) was referred to as Cases I and II respectively. As for the rectangular array, results referred to as Cases I, II and III represents setups seen in Figures 3.2(e), (f) and (g), respectively.

In order to provide basic intuition as to how the focusing behaves, the distribution of the electric field with the focal point placed in the origin ($x_f/\lambda = 0$) using Case I of the square array is given in Figure 4.1. All points in Figure 4.1 where $|\mathbf{E}(\mathbf{r})| < 0$ dBV/m were insignificant for the field's general characteristics and where therefore colored the same as $|\mathbf{E}(\mathbf{r})| = 0$ dBV/m to ease interpretation. This was also done for Figures 4.4 and 4.6.

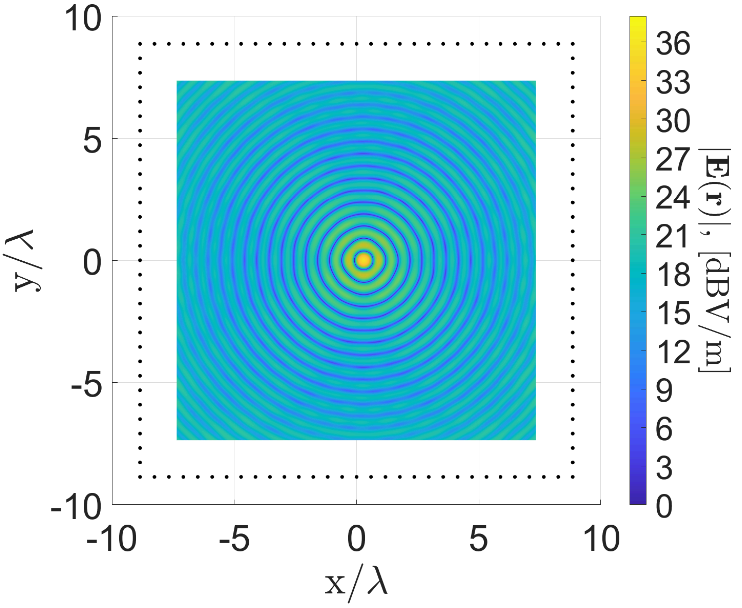

Figure 4.1: The electric field expressed in dBV/m when using Case I of the square array (depicted in Figure 3.2(c)) with $x_f/\lambda = 0$. As mentioned, the field closer than 1.5 λ from the array boundary is omitted.

4.1 Maximal electric field amplitude

The maximal achieved amplitude of the electric field for the different array configurations with equalized area can be seen in Figure 4.2. In all cases, the maximal amplitude of the field varied between 35 and 39 dBV/m. The highest maximal amplitude was found for the focal points closest to the array, and when approaching the center of the enclosed area, the field strength attenuated. The explanation for this behaviour was traced back to the fact that the electric field was inversely proportional to the distance from the radiator, as seen in (2.5).

When comparing the different arrays, it is evident that how high the amplitude is and how it changes when moving the focal point across the enclosed space is dependent on the array's shape. For example, the largest variation of the amplitude, $\approx$ 2.7 dBV/m, was found when using Case I of the square array and the smallest variation, $\approx$ 0.9 dBV/m was found when using Case I of the rectangular array.

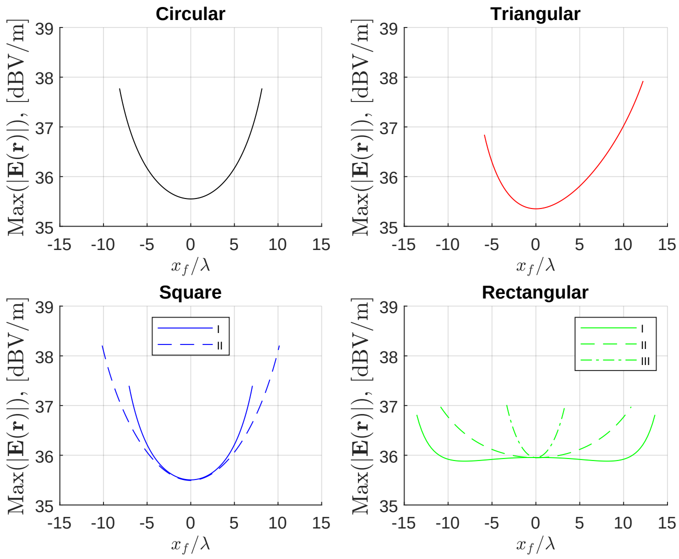

Figure 4.2: The maximal amplitude of the electric field expressed in dBV/m as the focal point is moved along the x-axis using arrays with equalized area. For the square array, Cases I and II refer to Figures 3.2(c) and (d), respectively, and for the rectangular array, Cases I, II and III refer to Figures 3.2(e), (f) and (g), respectively.

Case I of the rectangular array also differed in the aspect that it was the only configuration where there was no lowest point of amplitude in the middle of the enclosed area. Instead, for all focal points satisfying approximately $-10 < x_f/\lambda < 10$, the maximal amplitude was almost the same, 36 dBV/m. Notice how this was not the case for Cases II and III of the rectangular array. Therefore, it is concluded that one can expect to achieve similar amplitudes when moving the focal point parallel to the long sides of the rectangular array, but not when moving in different directions. One explanation for this characteristic is that, when far away from the short sides of the rectangular array, the distances to the closest antenna elements were similar when moving the focal point parallel to the long sides. Because of this it was reasonable to conclude that the electric field would be relatively similar for those points, since it was the closest elements that provided the greatest contributions to the electric field.

Due to the unique characteristic of this space, the size of the space was studied further. As can be seen in Case I of the rectangular array in Figure 4.2, there are two points where the amplitude is the smallest, and in between those points, the maximum amplitude changes little. The points where the smallest amplitude was found in was $x_f/\lambda = \pm 8.0$. Similar points were observed for the other ways of equalizing the arrays as well, and the distance between the points (l_c) divided by the total length of the long sides of the array (l_s) is presented in Table 4.1. Results in Table 4.1 allude to the region being almost half as long as the long sides of the arrays, despite the different areas and element separation of the arrays. From the results one could suspect that l_c is not strongly dependent on the area or element separation. Alternatively it is possible that it could have been more dependent on the ratio between the length of the long and short sides of the array. To confirm if that was the case would require more setups of rectangular arrays where the ratios between the sides are different, but this was left outside the scope of this study due to time constraints.

Equalizing:	Area	Aperture	Circumference
l_c/l_s	0.523	0.539	0.524

Table 4.1: Length of the region with little change (l_c) in $Max(|\mathbf{E}(\mathbf{r})|)$ divided by the total length of the long side of the rectangular array (l_s) in Case I for all three ways of equalizing the arrays.

When studying the square array in Figure 4.2, the maximal amplitude was not only dependent on the distance to the array, but also at what position in the enclosed space the focal point was placed in. For the square array, approaching the array along the diagonal, Case II, resulted in an increase of $\approx$ 1 dBV/m compared to if it was approached along the line of symmetry parallel to the sides, i.e, Case I. The same behaviour can also be seen when studying the triangular array. Moving the focal point in the direction of $-\mathbf{a}_x$ was similar to approaching a straight line of elements from a 90° angle, akin to that of Case I of the square array. When instead moving the focal point in the $\mathbf{a}_x$ direction the array was approached along an angle bisecting a corner of the triangle, which is more akin to Case II of the square array. The same behaviour gives indication that it is the same phenomenon that gave rise to the general trends. Specifically, when approaching a corner, there would be a larger number of elements in close proximity to the focal point. Therefore, higher amplitude of the electric field is expected.

With that behaviour identified, a peculiar result can be noticed when studying Case II of the rectangular array. In that case, the focal point was moved toward the corner of the array, but despite what happened for the square and triangular arrays, there is not as large of an increase in the electric field for the rectangular array. There is a slight increase in Case II compared to Case I of the rectangular array, $\approx 0.2 - 0.3$ dBV/m, but it was significantly smaller than the ≈ 1 dBV/m that was observed for the cases with the square and triangular arrays. A possible explanation for this could be that for Case II of the rectangular array, the corner was not approached along the corner's bisecting angle. Instead, it was approached with one angle to the array being $\approx 18.4°$, and the other being $\approx 71.6°$. This meant that one angle was ≈ 3.9 times larger than the other. For the Case II of the square array and the triangular array, both angles to the array was the same from the line of which the corner was approached. This resulted in the focal point not being as close to the corner for the rectangular array as it was for the square and triangular arrays. For Case II of the square array, the minimal distance between the focal point and the corner element was 2.38λ, while it was 5.32λ for Case II of the rectangular array. It is possible that this is the explanation as to why the same behavior was not captured for Case II of the rectangular array. If a simulation where the focal point is placed as close as possible to the corner of the rectangular array would have shown a large increase in the electric field, it would confirm that it was because of the differing lengths to the corner that the amplitude pattern differed.

No matter what method was used to equalize the arrays (see also results presented in Appendix A), the general pattern was the same when moving the focal point. The notable difference was in the maximal amplitude across all arrays, and how much it varied when moving the focal point. A smaller array resulted in higher amplitude with little variation, which is expected since the distances to the focal point from each element were smaller and changed less as the focal point was moved.

4.2 Size of the -3 dB spot region

The size of the -3 dB spot region for the different array configurations with equalized area can be seen in Figure 4.3. The length of the spot in the $\mathbf{a}_x$ and $\mathbf{a}_y$ directions ($l_x^{-3\text{dB}}$ and $l_y^{-3\text{dB}}$ respectively) are presented separately in subplots (a) and (b) of Figure 4.3. By first studying the results using the circular, triangular and square arrays, it can be identified that the spot was of about equal length in $\mathbf{a}_x$ and $\mathbf{a}_y$ for $x_f/\lambda = 0$, $l_x^{-3\text{dB}} \approx l_y^{-3\text{dB}} \approx 0.36\lambda$. For most cases when moving the focal point toward the array, the results show that $l_x^{-3\text{dB}}$ increase, while $l_y^{-3\text{dB}}$ decrease. This can be interpreted as when the focal point was close to the array, the -3 dB spot became elongated in the direction toward the array. For the circular, triangular and square arrays, $l_x^{-3\text{dB}}$ increased by ≈ 5 to 10 % and $l_y^{-3\text{dB}}$ decreased by only ≈ 5 %, depending on the array that was used. Cases I and II of the square array yield the smallest and largest change respectively. An important note when comparing Cases I and II for the squarearray is that $\mathbf{a}_x$ and $\mathbf{a}_y$ point toward the middle of the sides for Case I, while they point toward the corners in Case II. This explains the small difference in $l_x^{-3\text{dB}}$ and $l_y^{-3\text{dB}}$ for $x_f/\lambda = 0$.

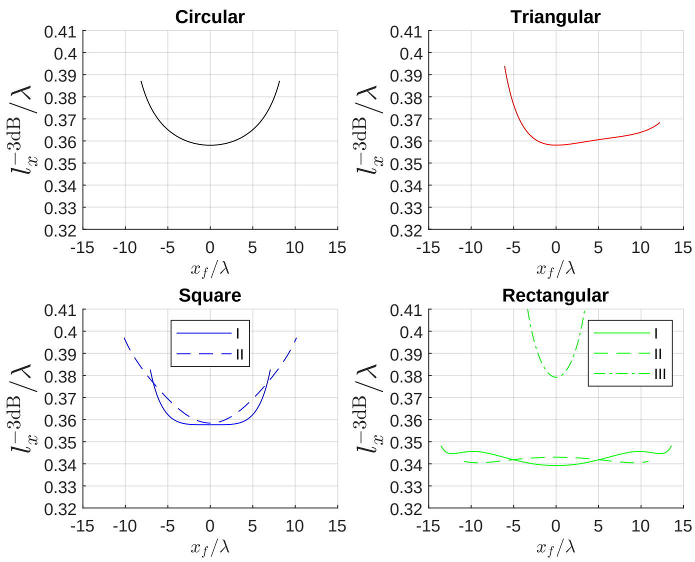

(a)

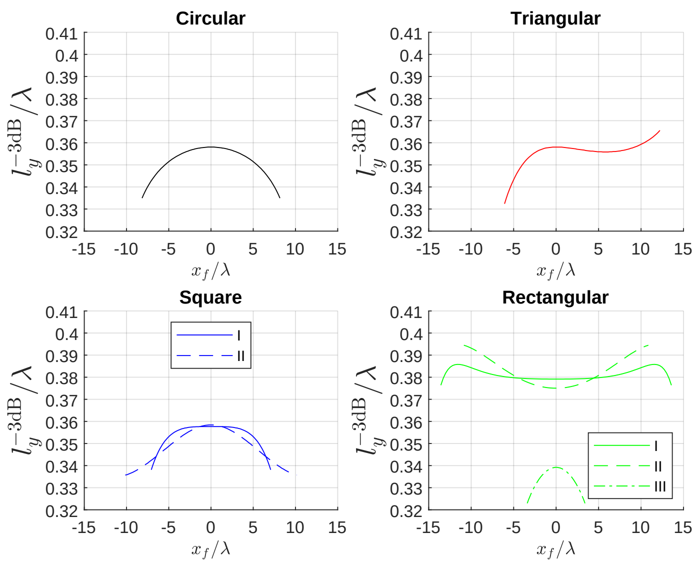

(b)

Figure 4.3: The size of the -3 dB spot region for the different array configurations with equalized area as the focal point was moved along the x-axis. The length in the $\mathbf{a}_x$ direction ($l_x^{-3\mathrm{dB}}$) is presented in (a), and the length in the $\mathbf{a}_y$ direction ($l_y^{-3\mathrm{dB}}$) is presented in (b).

When studying the circular, triangular and square arrays, there is one case where the pattern was not present. That is when approaching the corner of the triangular array. In that case, both $l_x^{-3\text{dB}}$ and $l_y^{-3\text{dB}}$ increased. Furthermore, they increased by similar amounts, ≈ 2 to 3 % compared to $x_f/\lambda = 0$. A comparison can be made between this result and Case II of the square array. In both cases, the corner of the array was approached along the bisecting angle, yet it was only for the triangular array that $l_y^{-3\text{dB}}$ increased. One possible explanation for the different results is that the angle of the corner for Case II of the square array was $90°$, while the angle of the corner for the triangular array was $60°$. On those grounds, a hypothesis describing how the spot was affected by the array geometry is proposed. When focusing near the array elements, the -3 dB spot region would be stretched toward the closest surrounding antenna elements. One can imagine that each antenna element is "pulling" the spot toward the element. That would have explained why, when approaching a straight line of elements, the spot was elongated toward the line, and when approaching a sharp angle, the spot was stretched in more than one direction, making the entire spot larger.

One important note is that the stretching resembles the concept of focal shift mentioned in [4] and [5]. In those experiments, a NFF array consisting of an array of antenna elements distributed in the xy-plane was studied as the focal point was moved along the z-axis. It was found that, when focusing using the conjugate-phase approach, the -3 dB spot region and position of the maximal amplitude of the electric field was shifted to a position closer to the antenna array than the chosen focal point. This was explained by the inverse proportionality between the electric field's amplitude and distance to the antenna elements. The stretching of the -3 dB spot that can be seen in Figure 4.3 behaved in a similar manner, as if the region was "pulled" toward the elements. Therefore, it is a possibility that the stretching of the -3 dB spot could be a result of the same phenomenon as for the focal shift presented in [4] and [5].

By studying the -3 dB spot for the rectangular array in Figure 4.3, the stretching of the spot is clearly demonstrated. For x_f far away from the short sides of the array, the spot is stretched toward the closest elements constituting the long sides of the array. The length in the direction pointing toward the long sides of the array can be seen Case III of the rectangular array in Figure 4.3(a) and in Case I of the rectangular array in Figure 4.3(b). For example, $l_x^{-3\text{dB}} = 0.34\lambda$ and $l_y^{-3\text{dB}} = 0.38\lambda$ for Case I. It is only when nearing the short sides of the array where the behavior started to resemble that of the other arrays. This is expected when considering the previous results, because the spot is stretched toward the closest elements. Despite this, the stretching is still strongest toward the long sides of the array for all tested x_f. One would have expected the stretching to be strongest toward the closest elements, but a possible explanation is that the large number of closely situated elements constituting the long sides of the array could have been dominant for this case.

The result from Case II of the rectangular array were more similar to that of Case I than Case III. This is also expected since the difference between Cases

II and I is that the array was rotated by $\approx 18.4°$, while the difference between Cases II and III is that the array was rotated by $\approx 71.6°$, being about 3.9 times as much. See Figure 3.2(e), (f) and (g) for clarification.

When comparing to the other ways of equalizing the arrays, the results were found to be nearly the same. There were no notable difference in the patterns of how $l_x^{-3\text{dB}}$ and $l_y^{-3\text{dB}}$ changed as the focal point was moved. There were some changes in how much the spot was stretched, but only to a degree that differed by ≈ 1 to 2 % to that presented in Figure 4.3.

Lastly it was worth noting that a maximal difference of 10% in $l_x^{-3\text{dB}}$ or $l_y^{-3\text{dB}}$, might not be significant enough to impact real life applications. Consider Figure 4.4, where the electric field is shown for the triangular array and four different focal points are chosen. The relatively small stretching of the focal region would be most noticeable by comparing (a) and (b), but because the change was only $\approx 10\%$, the general shape of the -3 dB spot was not drastically changed.

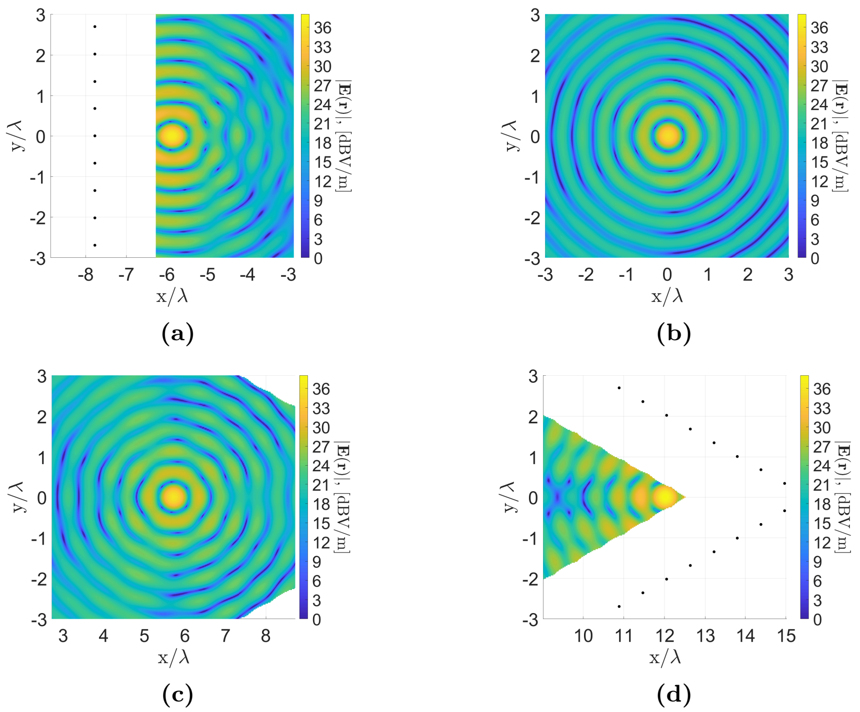

Figure 4.4: The electric field expressed in dBV/m when focusing at four different points in the enclosed space using the triangular array (depicted in Figure 3.2(b)), x_f/λ =-5.9 (a), 0.0 (b), 5.7 (c) and 12.0 (d).

4.3 SLL

The third way that the arrays were examined on was how high the highest sidelobe was compared to the maximal achieved amplitude. The SLL was studied by subtracting the highest sidelobe amplitude from the maximum amplitude, with the results presented in Figure 4.5. The largest difference in the SLL was found when using the circular array, where the main lobe was ≈ 7.9 dBV/m higher than the highest sidelobe. The triangular and rectangular arrays provided the smallest difference between the main lobe and the greatest sidelobe, ≈ 4.7 and ≈ 4.9 dBV/m.

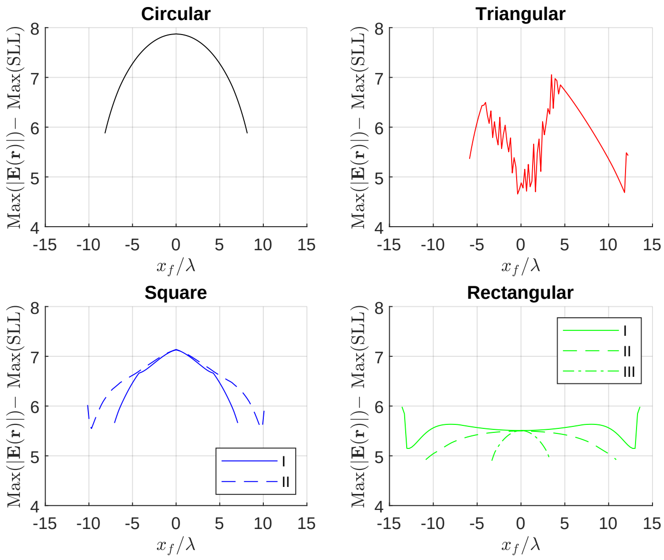

Figure 4.5: The SLL when moving the focal point along the x-axis of arrays with equalized area, expressed in dBV/m.

A pattern can be noticed when studying Figure 4.5. For most cases, the difference between the main lobe the highest sidelobe was greatest for $x_f/\lambda = 0$, and decreased as the focal point approached the array. How large this variation was depended on the array geometry, with the circular and triangular varying the most with ≈ 2 dBV/m and the cases for the rectangular array varying the least, ≈ 0.5 dBV/m. It should be noted that the variation for the triangular array was ≈ 2 dBV/m, which was significantly greater than for the rectangular, despite them both providing the lowest difference among the arrays with equalized area. The decreased difference was present despite the results shown in Figure 4.2, where the amplitude of the main lobe was shown to increase as the array was approached. From this it can be concluded that, as the focal point is moved toward the array, the amplitude of the greatest sidelobe increases faster than that of the main lobe.

Other than giving information on how the amplitudes differ, this conclusion also alludes to where the highest sidelobes most often were located. Figure 4.1 displays the electric field when simulating using Case I of the square array with $x_f/\lambda = 0$. Notice how high sidelobes were positioned closely around the main lobe. If this would have continued to be true as the focal point was moved toward, the sidelobes would most likely increase because of the inverse proportionality between the electric field and the distance to the elements. Since it was exactly this behaviour that can be seen in most of the results in Figure 4.5, it is likely that the highest sidelobes usually were positioned close to the main lobe, reinforced by results in Figures 4.4 and 4.6.

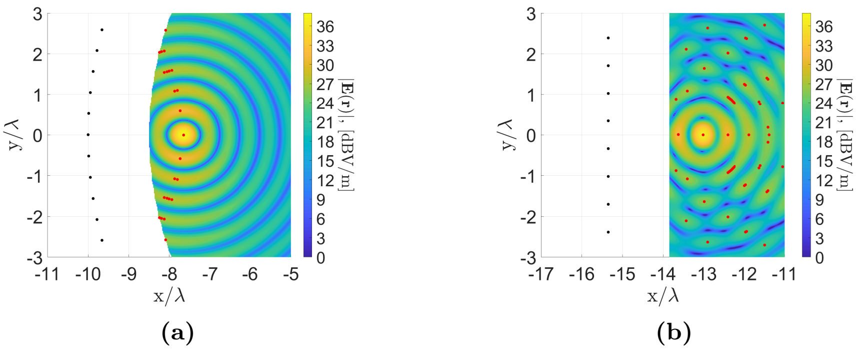

Figure 4.6: The electric field expressed in dBV/m when focusing close to the array for two configurations. (a) depicts the circular array (Figure 3.2(a)) with $x_f/\lambda = -7.65$ and (b) depicts Case I of the rectangular array (Figure 3.2(e)) with $x_f/\lambda = -13.0$. Local maxima of the amplitude are marked with red dots.

When studying the results in Figure 4.5, it can be noticed that for $x_f > 0$ for the triangular array, Case II of the square array and Case I for the rectangular array, the SLL changed rapidly when focusing close to the array. While this is unexpected, a possible explanation can be found by studying the electric fields in Figure 4.6. As can be seen on the marked local maxima, Figure 4.6(b) depicts that the sidelobe closest to the focal point was located along the x-axis for Case I of the rectangular array. The same was not true for the circular array, as can be seen by the local maxima in Figure 4.6(a). The orientation of the sidelobes would suggest that the high sidelobe to the left of the main lobe found in Figure 4.6(b) would cross the model's boundary when moving the focal point closer to the array, while the sidelobes in Figure 4.6(a) would not have be susceptible to the risk. This is a possible explanation as to why there was a sudden change in the SLL when close to the array in Case I of the rectangular array, while no such change was captured for the circular array, see Figure 4.5. If the highest sidelobe would be outside of the simulation area, it would not have been accounted for when Figure 4.5 was produced. Therefore, it is likely that the sudden change near the edge of the simulation space for $x_f > 0$ for the triangular array, Case II of the square array and Case I for the rectangular array was caused by the highest sidelobe leaving the simulation area. While results in Figure 4.2 may give a hint as to where the largest sidelobes form, further studies into where the sidelobes were formed would be necessary to properly understand their behaviour.

By specifically studying the triangular array in Figure 4.5, a peculiar behaviour can be discovered. For $-4.5 < x_f/\lambda < 4.5$ there were many sudden changes in the SLL. This is unexpected, but by studying Figure 4.7 a possible explanation can be found. Figure 4.7 depicted a slice along the x-axis of the electric field when using the triangular array and $x_f/\lambda = 0$. It shows that, other than a main lobe in $x = 0$, there was also a region with high amplitude near the tip of the array. The amplitude in this region was the highest sidelobe in the enclosed area, almost reminiscent of a grating lobe when doing far-field beamforming. The phenomenon is also likely connected to the fact that the element separation for the triangular array when equalizing the area was $d/\lambda = 0.67$, one of the largest found across all setups that was tested.

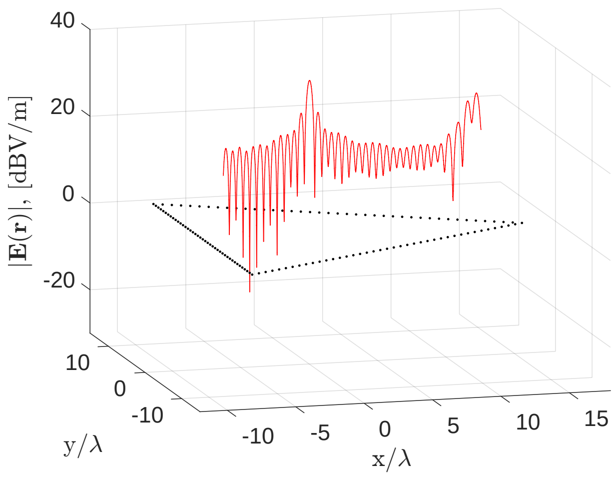

Figure 4.7: A slice of the electric field expressed in dBV/m along the x-axis when using $x_f/\lambda = 0$ for the triangular array when equalizing the area. The element separation for this array was $d/\lambda = 0.67$.

To further understand if it was due to the element separation that the space with high amplitude could form, the same array geometry was tested with the number of element increased to 150, which gave $d/\lambda = 0.54$. The results is shown in Figure 4.8. When studying Figure 4.8(b), the region near the tip of the triangular array does not display any significant increase in the SLL. This supported the connection between the grating lobe captured in Figure 4.7 and the sudden changes in the SLL seen in Figure 4.5. When studying Figure 4.8(a), a shape more akin to that of the other arrays in Figure 4.5 can be observed, further reinforcing the connection between the element separation, grating lobe and the unexpected region of high change in the SLL around $x_f/\lambda = 0$.

One note regarding the grating lobe captured using the triangular array was that it was the only case where such a sidelobe was identified. This was despite there was another array where the element separation was larger. The rectangular array had an element separation of $d = 0.68\lambda$, making it the largest of all array configurations. Yet it is only for the triangular array where the grating lobe is observed. Because of this it can be concluded that the forming of grating lobes is not only dependent on the element separation, but also the array's shape. One possibility is that there simply is not enough space enclosed by the rectangular array where the grating lobe could form. How the grating lobes are affected by the array's shape was not examined further in this study, but would be a relevant topic for future studies.

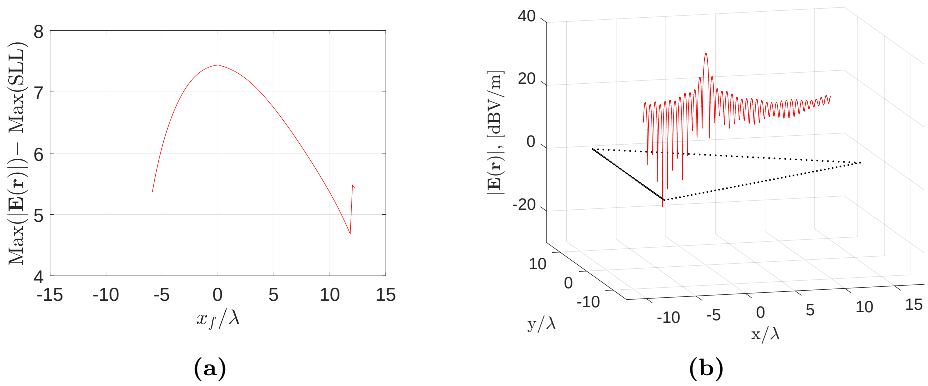

Figure 4.8: Results showing SLL from simulating the triangular array using $N = 150$ antenna elements ($d/\lambda = 0.54$) and equalizing the area. (a) The SLL for the triangular array. (b) A slice of the electric field along the x-axis when $x_f/\lambda = 0$. All amplitudes are expressed in dBV/m.

As for the other ways of equalizing the arrays, the results proved to be similar to that of equalizing the area. The only notable difference is that there was no grating lobe to be found when studying the triangular array. Since the area and element separation was smaller for the other methods of equalizing the arrays (see Table 3.1), it is to be expected that a grating lobe would not form.

Chapter 5

Summary

5.1 Conclusions

Four different 2D NFF antenna arrays have been studied in order to compare their performance using the conjugate-phase approach. The focusing point was placed on the enclosed planar space, and the maximal achieved electric field amplitude, size of the -3 dB spot region and SLL were studied.

For all arrays with equalized area, the maximal amplitude of the electric field was between 35 and 39 dBV/m. The achieved maximal amplitude of the electric field was the highest for points closest to the array in all cases. Specifically, it was the highest for points with many close antenna elements. This resulted in especially high amplitude near corners of arrays, with the highest amplitude found in the corner of the square array out of those with equalized area. The lowest amplitude was most often found in the center of the enclosed space. The exception to this is for Case I of the rectangular array, where instead there was very little change for approximately $-10 < x_f/\lambda < 10$. The smallest amplitude for this case was found for $x_f/\lambda = \pm 8.0$, with the region of little change being encapsulated by the lowest points. The largest variation in the amplitude of the electric field when choosing different focal points on the enclosed area was found using the square array, while the smallest was found on the rectangular array. These variations were ≈ 2.7 and ≈ 0.9 dBV/m respectively.

When studying the size of the -3 dB spot region, it can be observed that the length in the directions $\mathbf{a}_x$ and $\mathbf{a}_y$ was approximately the same for $x_f/\lambda = 0$ when using the circular, square and triangular arrays. The length of the spot in $\mathbf{a}_x$ and $\mathbf{a}_y$ was approximately 0.36λ in that case, $l_x^{-3\text{dB}} \approx l_y^{-3\text{dB}} \approx 0.36\lambda$. For x_f closer to the array, the spot was stretched toward the array. The stretching made at most a difference of $\approx 10\%$ in $l_x^{-3\text{dB}}$ and $l_y^{-3\text{dB}}$, with many cases being less than that. When near beside a straight line of elements, $l_x^{-3\text{dB}}$ increased while $l_y^{-3\text{dB}}$ decreased. For x_f close to the sharp corner in the triangular array, both $l_x^{-3\text{dB}}$ and $l_y^{-3\text{dB}}$ increased as elements close in both $\mathbf{a}_x$ and $\mathbf{a}_y$ was present. As for the rectangular array, the -3 dB spot was stretched even for $x_f/\lambda = 0$, making $l_x^{-3\text{dB}} = 0.34\lambda$ and $l_y^{-3\text{dB}} = 0.38\lambda$ for Case I. This is most likely because of the short distance to the long sides of the array. For x_f/λ near the short sides of the array, the region was stretched towards the short sides, but not to a degree where $l_x^{-3\text{dB}}$ ever was similar in length to $l_y^{-3\text{dB}}$. The stretching can be expected to be greater, to more closely resemble that of the other arrays, but it is a possibility that the large number of closely situated elements constituting the long sides of the array could offset the stretching toward the short side.

The SLL was at most $\approx$ 7.9 dBV/m, found using the circular array, while the lowest was $\approx$ 4.7 dBV/m, found using the triangular array. For different focal points using the same array, the difference varied between $\approx$ 2 dBV/m and $\approx$ 0.5 dBV/m, with the highest variation being found for the circular array, and the lowest being found for the rectangular array. By combining results regarding the SLL with information regarding the entire electric field for a specified x_f/λ, it can be concluded that the highest sidelobe was situated close to the main lobe in almost all cases. The exception to this is for the triangular array, where for $-4.5 < x_f/\lambda < 4.5$, large sidelobes appeared at the corners of the array. Due to the large element separation of the triangular array, and unusual character of the sidelobes, the phenomenon is likely related to that of grating lobes in the far-field context. By simulating using a larger number of elements, thus lowering the element separation, it was found that the largest sidelobes had disappeared, reinforcing the hypothesis that the phenomenon is connected to grating lobes.

While the different array geometries resulted in different characteristics for the focusing, the explanation behind the characteristics can often be traced back to the inverse proportionality between the electric field and the distance to the antenna elements. It is also noted that how much the maximal amplitude, size of the -3 dB spot region and SLL change for different focal points followed a pattern for the arrays. For the circular array, higher variation for all studied attributes was captured than for the rectangular array. From the pattern it can be concluded that if there were large variations in either the maximal amplitude, size of the -3 dB spot or the SLL, the other attributes can also be expected to vary. Since all attributes seemed to relate to the inverse proportionality between the amplitude of the electric field and distance to the closest elements, one can expect to see larger variations for the studied aspect when the distance to the closest elements vary more. This claim is further supported by comparing with results found in Appendix A, where the arrays had been equalized using other methods, resulting in different area and circumference. For arrays where the enclosed space was smaller, less variation in all studied attributes can be observed. Therefore it can be concluded that arrays which resulted in large possible variation in the distance between the focal point and the closest antenna elements, can also result in large variation regarding the aspects the performance was evaluated by.

Yet, all the studied aspects were comparable when regarding the arrays with equalized area. The maximal amplitude varied at most by 2.7 dBV/m, and SLL no more than 3 dBV/m between the geometries. The size of the -3 dB spot varied little as well. This shows that despite the use of different geometries, all shapes can be considered to be valid options when used for NFF arras focus in the enclosed 2D space.

By comparing the results from arrays with different area and circumference found in Appendix A, it can also be observed that for arrays with smaller area and circumference, the resulting maximal amplitude was higher, while the size of the -3 dB spot was relatively unchanged. The amplitude of the sidelobes were also increased for the smaller arrays, but the difference between the maximal amplitude and the highest sidelobe was still similar for all the ways the arrays were equalized. The exception to this is for the triangular array using equalized area, where grating lobes formed.

5.2 Possible future work

With the above mentioned results and conclusions drawn, there are parts of the study that can be improved upon. The impact of corners in the array is one of the topics deserving of more attention. As it stands, one could choose between the circular and rectangular array in order to achieve better but more varied, or worse but more consistent performance. Studies examining different ways of distributing the antenna elements to achieve good and consistent performance would be of value in hopes of finding the optimal array shape. It can be seen that the maximal amplitude and -3 dB spot were affected greatly by how sharp the corner was, and from what direction it was approached. By studying differently angled corners, and approaching them from different directions, it would been possible to better understand exactly how the performance would be affected. There are also still questions left regarding the forming of the sidelobes, both the SLL and at what positions they form. It can be seen that the greatest sidelobe often was formed near the focal point, but there are no conclusion drawn as to on what side of the focal point the highest peak was. This, along with when and where the grating lobes appear, would be good to understand to better prepare for future endeavours in constructing wireless communication systems using NFF arrays in a LIS-context.

Other aspects worth studying in future research include how the electric field behaves in the reactive near-field, how the performance could be increased further through incorporating weighted amplitudes and the use of optimization algorithms and how similar arrays perform in 3D space. With the knowledge acquired from such studies, challenges and opportunities for real-life application of LIS for wireless communication would be identified and used to further tackle future requirements for high data rates and wireless energy transfer.

References

[1] H. Asplund, D. Astely, P. Butovitsch, T. Chapman, M. Frenne, F. Ghasemzadeh, M. Hagström, B. Hogan, G. Jöngren, J. Karlsson, F. Kronestedt and E. Larsson, *Advanced Antenna Systems for 5G Network Deployments*, London, United Kingdom: Academic Press, 2020.

[2] D. K. Cheng, *Field and Wave Electromagnetics*, 2nd. ed, Harlow, United Kingdom: Pearson Education Limited, 2013.

[3] W. Gosling, *Radio Antennas and Propagation*, Oxford, United Kingdom: Newnes, 1998.

[4] P. Nepa and A. Buffi, "Near-field-focused microwave antennas: Nearfield shaping and implementation," *IEEE Antennas Propag. Mag.*, vol. 59, no. 3, pp. 42-53, June 2017.

[5] A. Buffi, P. Nepa, and G. Manara, "Design criteria for near-field-focused planar arrays," *IEEE Antennas Propag. Mag.*, vol. 54, no. 1, pp. 40-50, Feb. 2012.

Appendix A

Results from using different ways of equalizing the arrays

Detailed results from simulations using the alternative ways of equalizing the arrays are presented in this appendix. The focus of the study is not on the results presented in this appendix. Therefore, the results for the alternative ways of equalizing the arrays are only presented here, not analyzed. The analysis done on these results can be found in Chapters 4 and 5 of the study, *Results and discussion* and *Summary*. Like that of the main text, in order to distinguish results from simulations using the same array, using the square array setups seen in Figure 3.2(c) and (d), the results are referred to as Cases I and II, respectively. As for the rectangular array, results are referred to as Cases I, II and III represent setups seen in Figure 3.2(e), (f) and (g), respectively.

A.1 Equalizing the aperture

By equalizing the aperture, the longest length found across the array was equalized. The arrays can be seen in Figure A.1. The results using this method of equalization is presented in this section. Figure A.2 shows the maximal amplitude of the electric field as the focal point was moved along the x-axis, akin to that of Figure 4.2. The size of the -3 dB spot region when equalizing the aperture can be found in Figure A.3. The results correspond to those presented in Figure 4.3, with (a) depicting the length in $\mathbf{a}_x$ ($l_x^{-3\text{dB}}$) and (b) depicting the length in $\mathbf{a}_y$ ($l_y^{-3\text{dB}}$) for the different cases. Figure A.4 shows the SLL, corresponding to Figure 4.5. Finally, Figure A.5 shows a slice along the x-axis when using the triangular array and $x_f/\lambda = 0$, the same case as for Figure 4.7 but when equalizing the aperture.

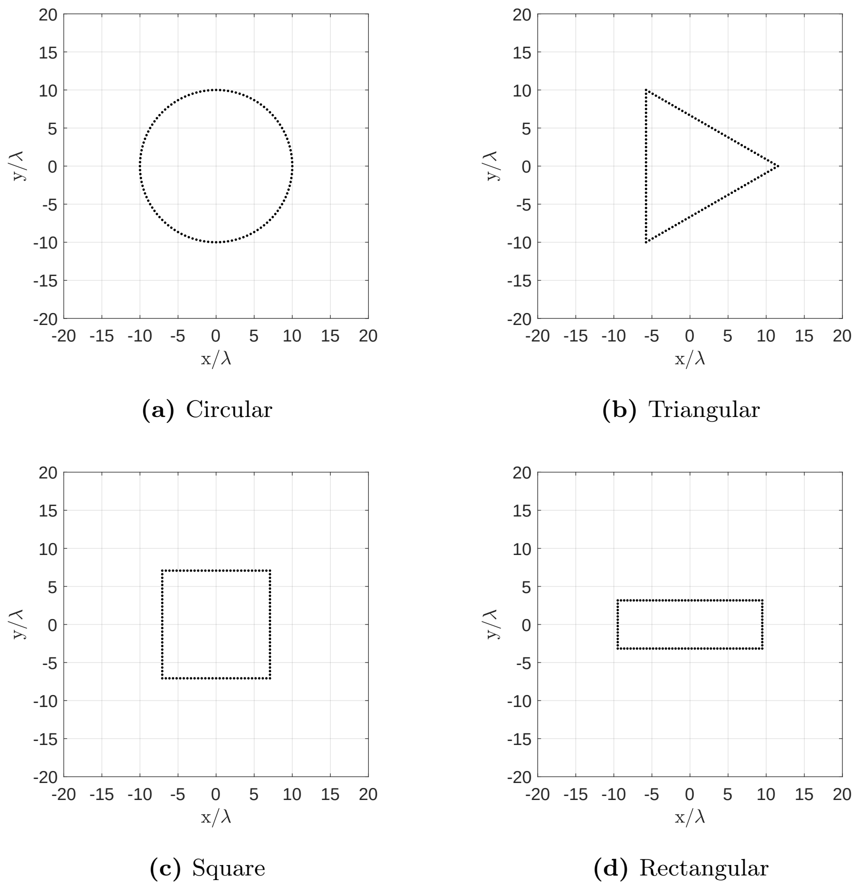

(a) Circular **(b)** Triangular

(c) Square **(d)** Rectangular

Figure A.1: Planar arrays with equalized aperture consisting of $N = 120$ elements each, marked with black dots. The x and y coordinates of each element is scaled to the wavelength.

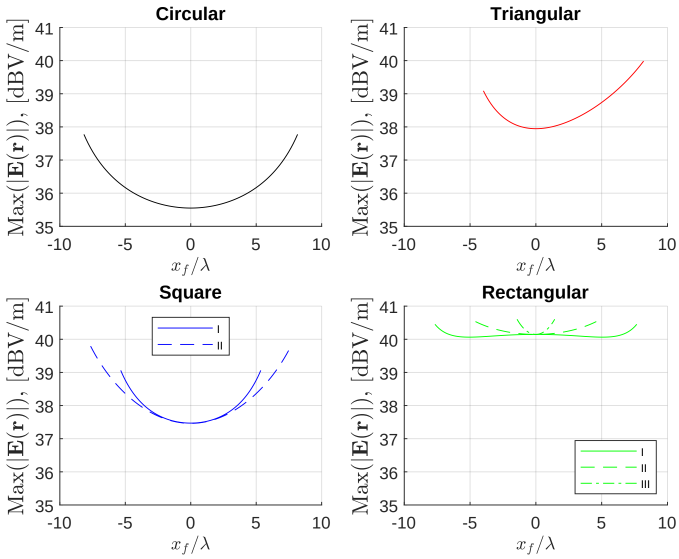

Figure A.2: The maximal amplitude of the electric field expressed in dBV/m as the focal point is moved along the x-axis using arrays with equalized aperture.

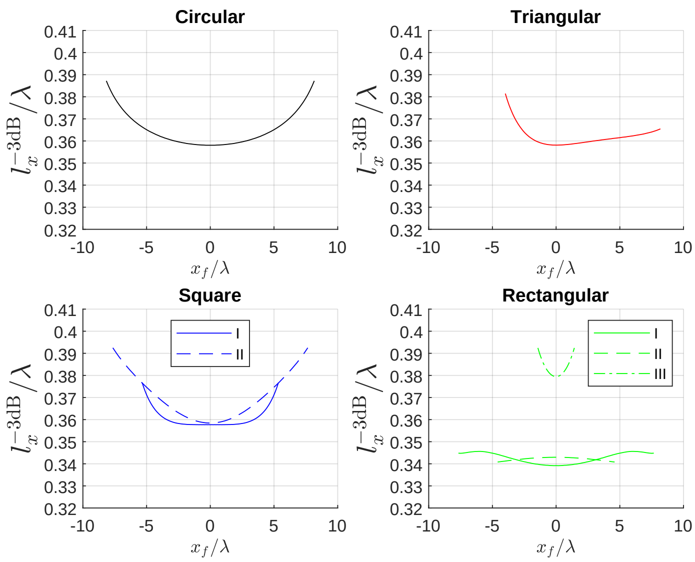

(a)

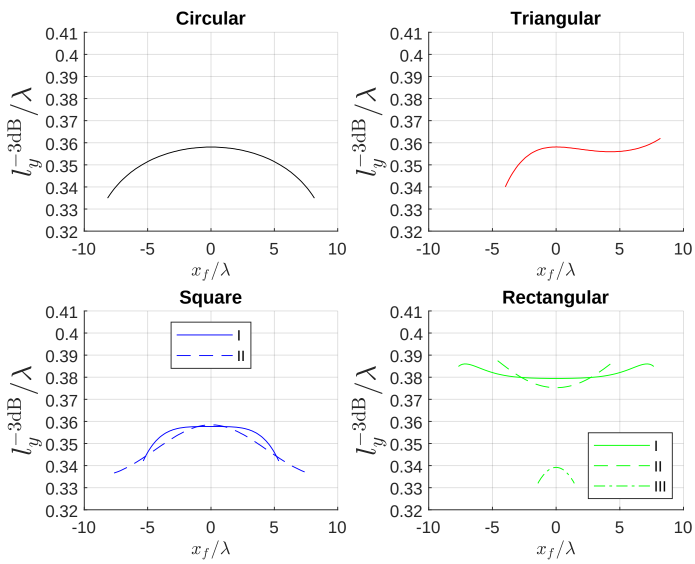

(b)

Figure A.3: The size of the -3 dB spot region for the different array configurations with equalized aperture as the focal point was moved along the x-axis. The length in the $\mathbf{a}_x$ direction ($l_x^{-3\mathrm{dB}}$) is presented in (a), and the length in the $\mathbf{a}_y$ direction ($l_y^{-3\mathrm{dB}}$) is presented in (b).

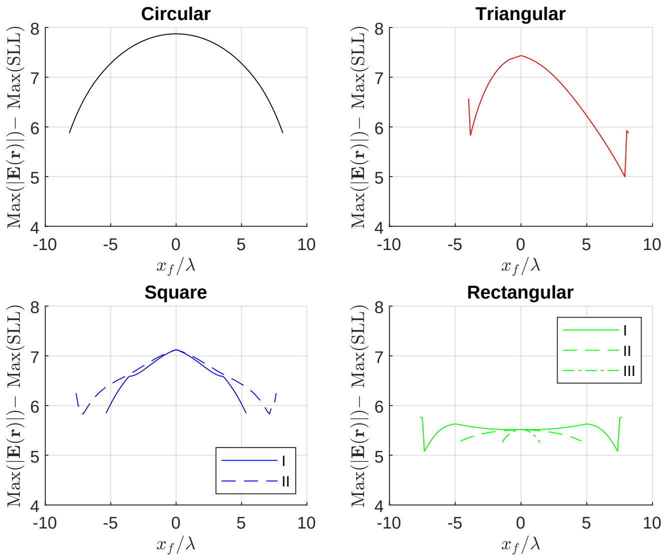

Figure A.4: The SLL when moving the focal point along the x-axis of arrays with equalized aperture, expressed in dBV/m.

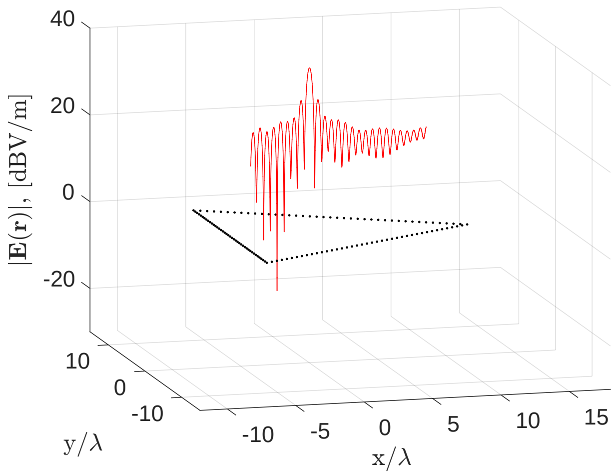

Figure A.5: A slice of the electric field expressed in dBV/m along the x-axis when using $x_f/\lambda = 0$ for the triangular array when equalizing the aperture. The element separation for this array was $d/\lambda = 0.5$.

A.2 Equalizing the circumference

By equalizing the circumference, the element separation was the same for all arrays. The arrays can be seen in Figure A.6. The results using this method of equalization is presented in this section. They were presented in a similar way as for section A.1. Figure A.7 shows the maximal amplitude of the electric field as the focal point was moved along the x-axis, akin to that of Figure 4.2. The size of the -3 dB spot region when equalizing the circumference can be found in Figure A.8. The results correspond those presented in Figure 4.3, with (a) depicting the length in $\mathbf{a}_x$ ($l_x^{-3\text{dB}}$) and (b) depicting the length in $\mathbf{a}_y$ ($l_y^{-3\text{dB}}$) for the different cases. Figure A.9 shows the difference between the maximal amplitude of the electric field and the highest amplitude of the sidelobes, corresponding to Figure 4.5. Finally, Figure A.10 shows a slice along the x-axis when using the triangular array and $x_f/\lambda = 0$, the same case as for Figure 4.7 but when equalizing the circumference.

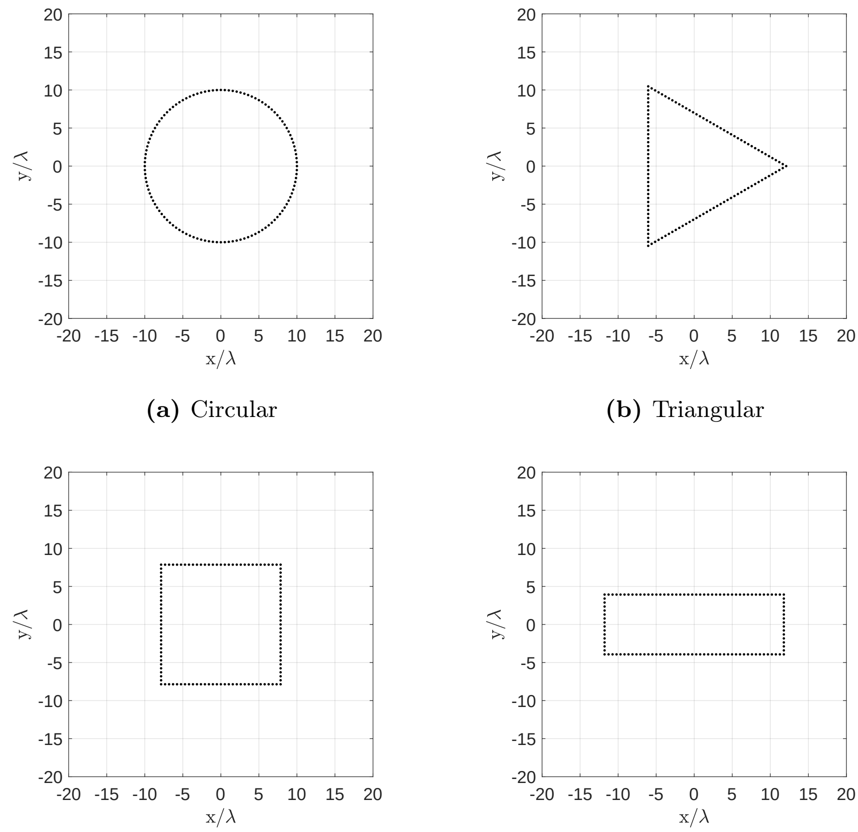

(a) Circular **(b)** Triangular

(c) Square **(d)** Rectangular

Figure A.6: Planar arrays with equalized circumference consisting of $N = 120$ elements each, marked with black dots. The x and y coordinates of each element is scaled to the wavelength.

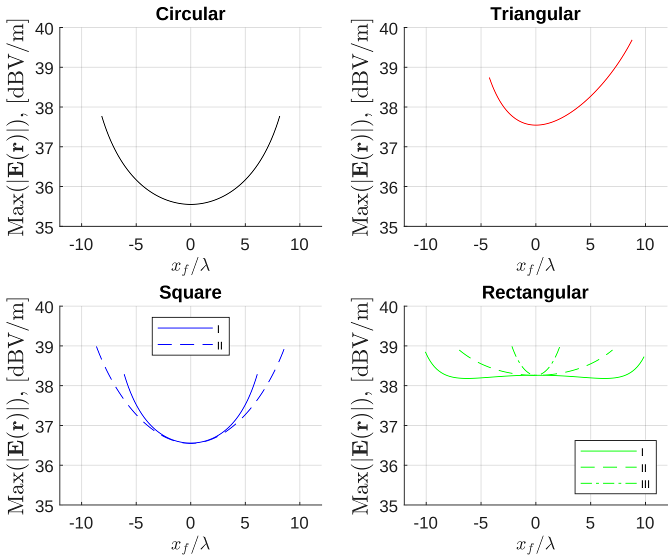

Figure A.7: The maximal amplitude of the electric field expressed in dBV/m as the focal point is moved along the x-axis using arrays with equalized circumference.

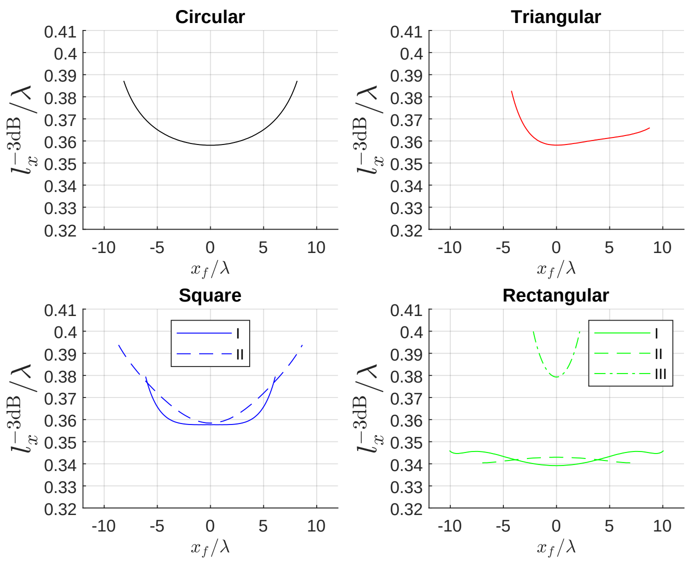

(a)

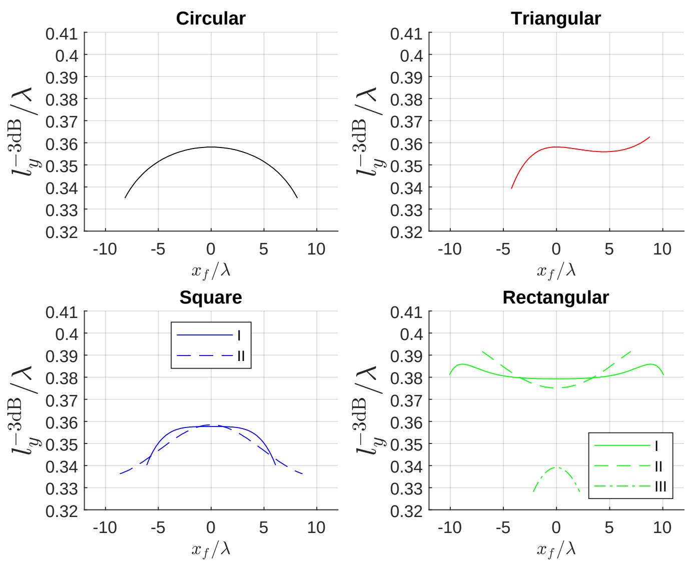

(b)

Figure A.8: The size of the -3 dB spot region for the different array configurations with equalized circumference as the focal point was moved along the x-axis. The length in the $\mathbf{a}_x$ direction ($l_x^{-3\mathrm{dB}}$) is presented in (a), and the length in the $\mathbf{a}_y$ direction ($l_y^{-3\mathrm{dB}}$) is presented in (b).

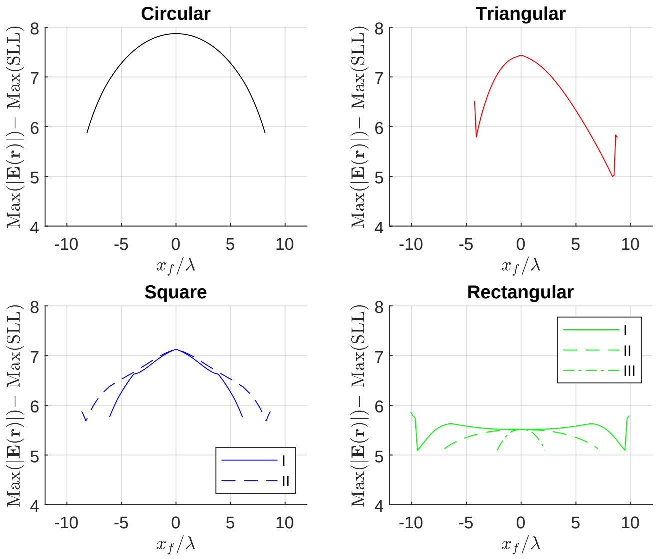

Figure A.9: The SLL when moving the focal point along the x-axis of arrays with equalized circumference, expressed in dBV/m.

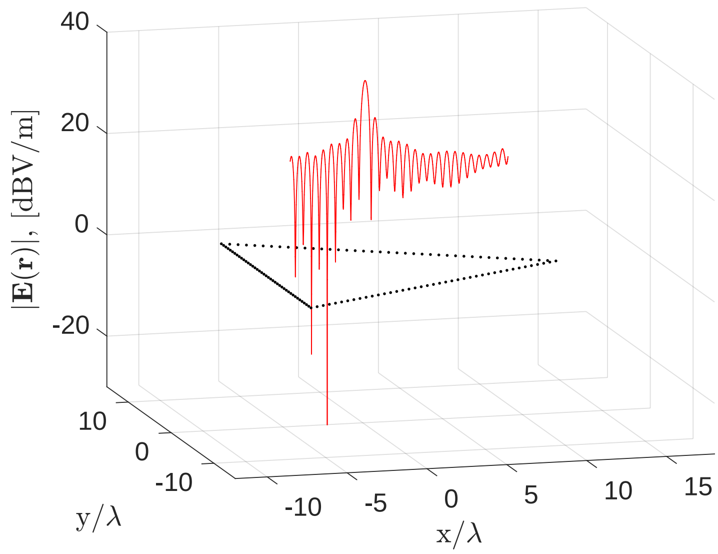

Figure A.10: A slice of the electric field expressed in dBV/m along the x-axis when using $x_f/\lambda = 0$ for the triangular array when equalizing the circumference. The element separation for this array was $d/\lambda = 0.52$.

Printed by Tryckeriet i E-huset, Lund 2024

LUND
UNIVERSITY

Series of Master´s theses
Department of Electrical and Information Technology
LU/LTH-EIT 2024-1026
http://www.eit.lth.se